Supplementary materials

Tunable Topological Phases in a New Natural $MnSb_2Te_4/(Sb_2Te_3)_2$ superlattice

X. Zhang[1,8], S.H. Zhang[1,8], Z.C. Jiang[2,8], S. C. Huan[1], Yichen Yang[2], Zhengtai Liu[2], Song Yang[3], Jinlong Jiao[4], Litao Yu[3], Wei Xia[1,5], Xia Wang[1,6], Na Yu[1,6], Zhiqiang Zou[1,6], Yongsheng Liu[3], Jie Ma[4], Dawei Shen[2,7,*], Jianpeng Liu[1,5,*], and Y. F. Guo[1,5,*]

[1] School of Physical Science and Technology, ShanghaiTech University, Shanghai 201210, China
[2] State Key Laboratory of Functional Materials for Informatics, Shanghai Institute of Microsystem and Information Technology (SIMIT), Chinese Academy of Sciences, Shanghai 200050, China
[3] Institute of Solar Energy, Shanghai University of Electric Power, Shanghai 200090, China
[4] Key Laboratory of Artificial Structures and Quantum Control (Ministry of Education), School of Physics and Astronomy, Shanghai Jiao Tong University, Shanghai 200240, China
[5] ShanghaiTech Laboratory for Topological Physics, ShanghaiTech University, Shanghai 201210, China
[6] Analytical Instrumentation Center, School of Physical Science and Technology, ShanghaiTech University, Shanghai 201210, China
[7] Center of Materials Science and Optoelectronics Engineering, University of Chinese Academy of Sciences, Beijing 100049, China
[8] These authors contributed equally: X. Zhang, S. H. Zhang, J. C. Jiang.

* Corresponding author.
E-mail address: guoyf@shanghaitech.edu.cn (Y. F. Guo), liujp@shanghaitech.edu.cn (J. P. Liu), dwshen@mail.sim.ac.cn (D. W. Shen).

Supplementary Note 1: The magnetization characterizations

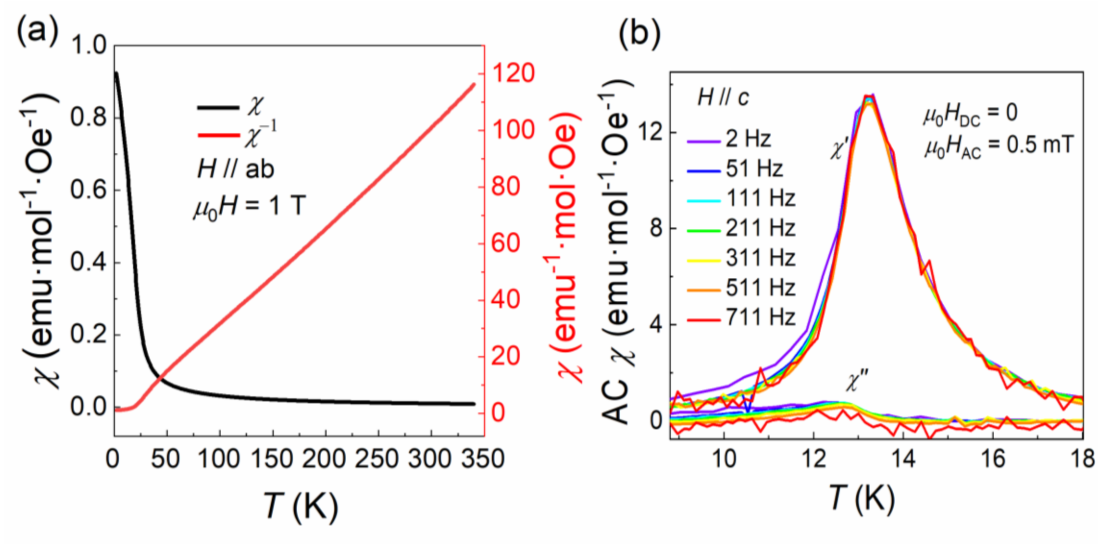

Fig. S1. (a) The temperature dependent magnetic susceptibility χ and reciprocal magnetic susceptibility χ^{-1} under μ_0H = 1 T for *H* // *ab* plane. (b) AC susceptibility for $MnSb_2Te_4/(Sb_2Te_3)_2$ at frequencies between 2 and 711 Hz.

The Curie-Weiss law was used to fit the reciprocal magnetic susceptibility χ^{-1} of $MnSb_2Te_4/(Sb_2Te_3)_2$ between 50 K to 350 K measured with μ_0H = 1 T and *H*//*ab* plane, shown in Fig. S1a, which gives the Weiss temperature θ_w = 11.09 K and the effective moment μ_{eff} = 4.54 μ_B/Mn. The effective moment is close to the expected 5 μ_B for the Mn^{2+} ion. The positive Weiss temperature indicates the FM ground state of $MnSb_2Te_4/(Sb_2Te_3)_2$, which is also supported by the clear hysteresis loop in *M*(*H*) as shown in Fig. 1d of the main text. The ac magnetic susceptibility measured at μ_0H_{AC} = 0.5 mT at different frequencies for *H*//*c* is presented in Fig. S1b, which apparently shows no frequency dependence.

As mentioned in the main text, the long range AFM order in $MnSb_2Te_4/(Sb_2Te_3)_2$ could be identified in the magnetic susceptibility curves at T_N = 12.7 K. When *H*//*c*, the ZFC and FC curves show clear separation at low temperature, indicating the possibility of hysteresis loops signifying the ferrimagnetic or FM state, demonstrated by the hysteresis loops of isothermal magnetizations as shown in Fig. S2c, where a first-order spin-flop transition with hysteresis at 4 K beginning around μ_0H = 30 mT and vanishing at μ_0H = 40 mT is visible, indicating very soft magnetism. It is also clear that though the magnetic ground state is FM, it is fragile and becomes ferrimagnetic or AFM at higher temperature. However, at μ_0H = 40 mT, the ferrimagnetic state also enters into the induced spin-polarized FM state. Comparing with the $MnSb_2Te_4$ and $MnSb_2Te_4/Sb_2Te_3$[1,2], the smaller saturation magnetic field of $MnSb_2Te_4/(Sb_2Te_3)_2$ indicates the weaker Mn^{2+} - Mn^{2+} interlayer AFM exchange. While increasing the temperature to 15 K, the hysteresis loop as well as the spin-flop transition gradually diminishes. The saturation moment at 2 K under μ_0H = 0.1 T is 1.7 μ_B/Mn^{2+}, which is smaller than the value of 1.93μ_B/Mn^{2+} of $MnSb_2Te_4/Sb_2Te_3$[2]. The remarkably reduced magnetic moment may due to that the Mn disorders and mixed location of Mn and Sb atoms[3], or is caused by the enhanced hole-carrier mediated Ruderman-Kittle-Kasuya-Yosida (RKKY) interaction which could give rise to magnetic frustration[4-6]. Fig. S2a,b display the isothermal magnetizations with *H*//*c* and *H*//*ab*, showing apparently that the saturation field for *H*//*c* is slightly smaller than that for *H*//*ab* at the same temperature, which indicates that the *c* axis is still the magnetic easy axis for $MnSb_2Te_4/(Sb_2Te_3)_2$.

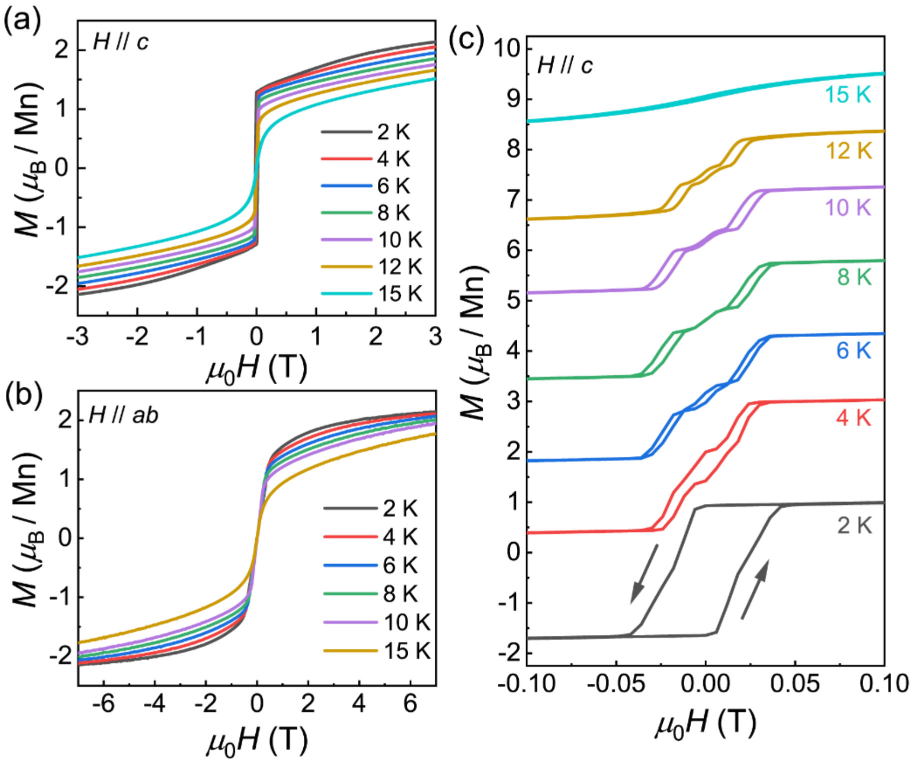

Fig. S2. (a,b) The isothermal magnetizations of $MnSb_2Te_4/(Sb_2Te_3)_2$ at various temperatures with $H//c$ axis and $H//ab$ plane, respectively. (c) The hysteresis loop of isothermal magnetizations at various temperatures with $H//c$ axis.

Supplementary Note 2: The calculated surface states in the AFM state and anomalous Hall conductivities

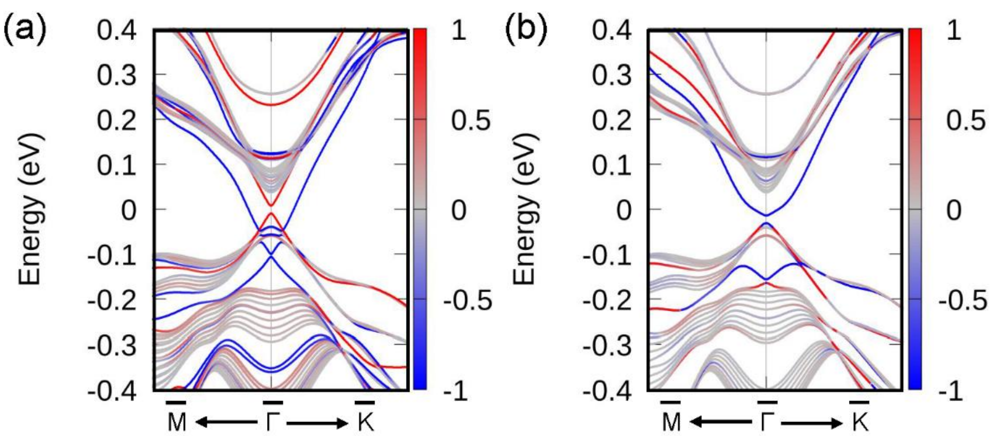

Fig. S3. The surface states in the AFM configuration. (a) The red lines refer to the surface states originated from SL-QL-QL... termination, and the blue lines represent the surface states from QL-QL-SL... surface. In (b), two types of surfaces states are both for the QL–SL–QL...

surface. Here the Fermi level is set to zero and the bulk states are remarked by gray lines. It can be seen that the surface states in the AFM state is similar to those in the FMz state.

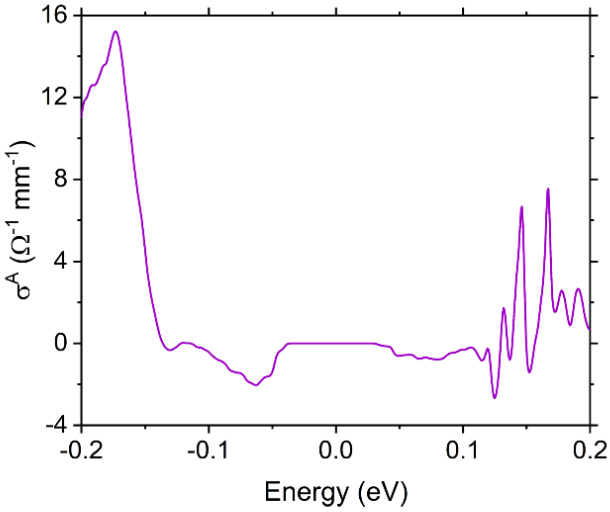

Fig. S4. The calculated anomalous Hall conductivities of $MnSb_2Te_4/(Sb_2Te_3)_2$ in the FMz state. Here the Femi energy is set as zero. The calculated AHC at the -382 meV is 2.05 Ω^{-1} mm^{-1} which is close to experimental value.

Table S1. The positions and chiralities of Weyl nodes near the Fermi level in the valence bands in the FMz phase. Here the bands are remarked by VB, VB-1, VB-2… from the highest valence band to lower valence band.

Weyl nodes (ang^{-1})	band	chirality
(-0.182, 0.106, -0.013)	VB-2 and VB-3	1
(0.182, -0.106, 0.013)	VB-2 and VB-3	-1
(0.000, -0.210, -0.013)	VB-2 and VB-3	1
(0.000, 0.210, 0.013)	VB-2 and VB-3	-1
(-0.206, 0.119, 0.001)	VB-3 and VB-4	-1
(0.206, -0.119, -0.001)	VB-3 and VB-4	1

As we discussed in the main text, the Wilson loops presented in Fig. 2f indicate nontrivial topological states in the FMz state and the Z_4 = 2 means an axion insulator of the FMz $MnSb_2Te_4/(Sb_2Te_3)_2$. Similar as the case in AFM $MnSb_2Te_4/(Sb_2Te_3)_2$ presented in Fig. S3a,b, the SL–QL–QL... A-type surface of surface is terminated with SL layer and hence has a gapped Dirac band dispersion, while the QL–QL–SL... B-type surface is with the surface states throughout the bulk gap and makes the system metallic at the surface. The calculated intrinsic AHC at 2 K is presented in Fig. S4, showing a value that is consisteng with the experimnental one. To know more details about the Weyl state in the FM phase, the calculated positions and chiralities of Weyl nodes near the Fermi level in the valence bands are summarized in Table S1.

Supplementary Note 3: The complementary magneto-transport data

The magnetic field dependent $\rho_{xx}(H)$ and $\rho_{xy}(H)$ of $MnSb_2Te_4/(Sb_2Te_3)_2$, measured in the magnetic field range of μ_0H = -9 T - 9T are shown in Fig. S5a,b, respectively. In Fig. S4a, the $\rho_{xx}(H)$ curves exhibit an overall "M" shape, which is possibly caused by the combination of nonmagnetic parabolic magnetoresistance (MR) and negative MR due to FM fluctuations. It is also clear that the M-shaped MR almost disappears and becomes a parabolic shape above T_N, suggesting the rather weak FM fluctuations above the T_N in $MnSb_2Te_4/(Sb_2Te_3)_2$, which resembles the case of $MnBi_2Te_4/(Bi_2Te_3)_3$ superlattice[7]. The magnetotransport properties are tightly related with the magnetic structure. As displayed in Fig. S6, $\rho_{xx}(H)$ follows the same hysteresis loop as that in $M(H)$ with $H//c$ and $I//ab$ plane, where the red and black arrows represent the paths for changing the magnetic field. The clear hysteresis loop without the multiple transitions feature indicates the FM ground state of $MnSb_2Te_4/(Sb_2Te_3)_2$.

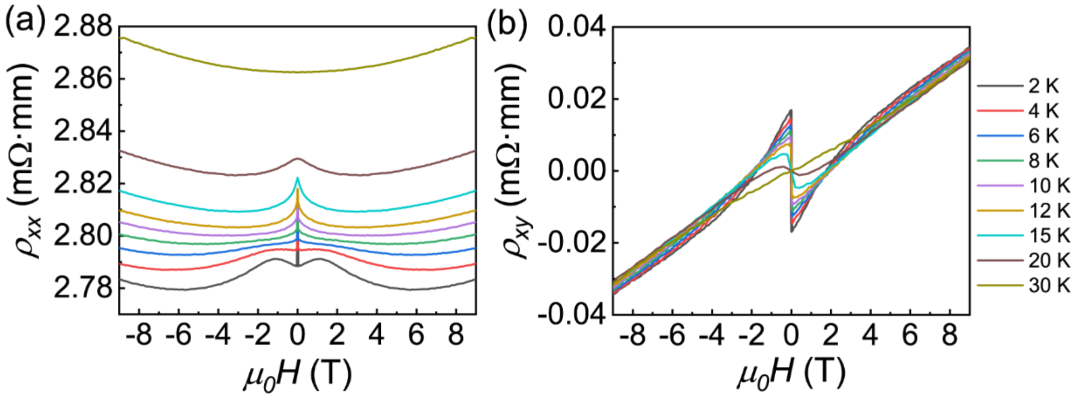

Fig. S5. Magnetotransport properties of bulk $MnSb_2Te_4/(Sb_2Te_3)_2$. (a) Magnetoresistance ρ_{xx} with $I//ab$ plane and $H//c$ axis at various temperatures. (b) Hall resistivity ρ_{xy} measured at the same temperatures as in (a).

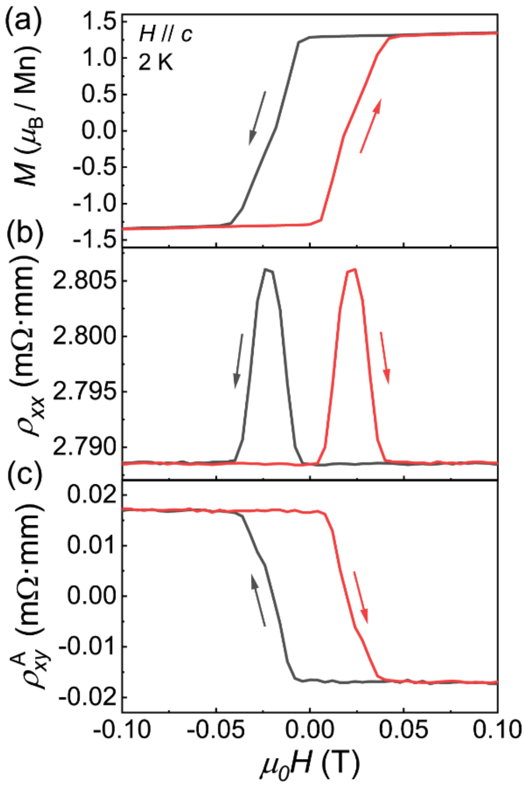

Fig. S6. Magnetotransport properties of bulk $MnSb_2Te_4/(Sb_2Te_3)_2$ superlattice. (a) The field dependence of magnetization *M*. (b) transverse magnetoresistance ρ_{xx}. (c) anomalous Hall resistivity ρ_{xy}^{A} at 2 K with *H*//*c* and *I*//*ab* plane.

Supplementary Note 4: ARPES measurements of pure and Bi doping $MnSb_2Te_4/(Sb_2Te_3)_2$

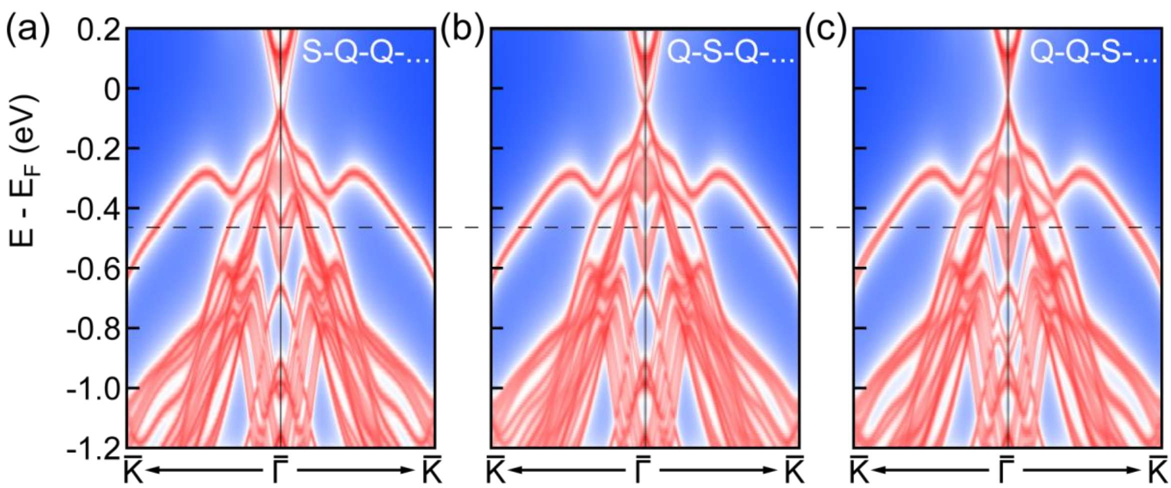

Fig. S7. Calculation comparision of three kinds of termination along $\bar{K}$-$\bar{\Gamma}$-$\bar{K}$ direction of $MnSb_2Te_4/(Sb_2Te_3)_2$. (a) SL-QL-QL-... termination. (b) QL-SL-QL-... termination. (c) QL-QL-SL-... termination. Experimental Fermi level is marked by dark dash line.

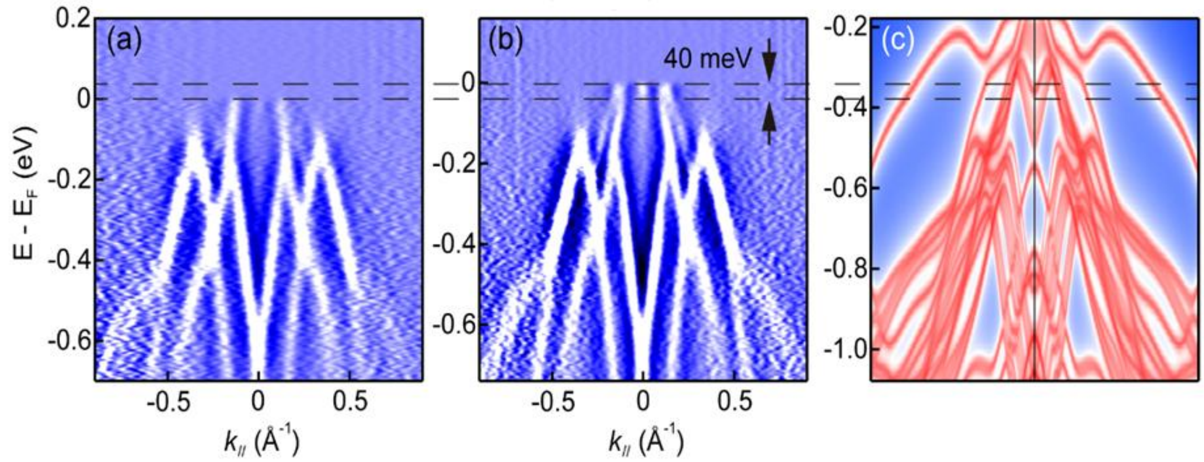

Fig. S8. ARPES measurements of pure and Bi doping $MnSb_2Te_4/(Sb_2Te_3)_2$ and $Mn(Bi_{0.2}Sb_{0.8})_6Te_{10}$ single crystal. (a) ARPES results of pure $MnSb_2Te_4/(Sb_2Te_3)_2$ along $\bar{K}$-$\bar{\Gamma}$-$\bar{K}$ direction. (b) ARPES results of $Mn(Bi_{0.2}Sb_{0.8})_6Te_{10}$ along $\bar{K}$-$\bar{\Gamma}$-$\bar{K}$ direction. (c) DFT calculation of $MnSb_2Te_4/(Sb_2Te_3)_2$ along $\bar{K}$-$\bar{\Gamma}$-$\bar{K}$ direction.

To further resolve these Dirac surface states, the calculated surface states along the $\bar{K}$-$\bar{\Gamma}$-$\bar{K}$ direction for the three difefrent termionations in Fig. S7 are presented, which clearly show that their band structure is in fact indistinguishable near E_F. Therefore, by ARPES measurement, the existence of non-trivial topological surface states is confirmed in $MnSb_2Te_4/(Sb_2Te_3)_2$. We tried to tune its chemical potential by Bi substitution for Sb in $MnSb_2Te_4/(Sb_2Te_3)_2$ as well as by alkali metal doping. As shown in Fig. S8, with 20% Bi substitution as $Mn(Bi_{0.2}Sb_{0.8})_6Te_{10}$, the E_F shifts upward by approximately 40 meV. At the same time, the multi bulk bands marked by green arrows in Fig. 4e,f become much clearer. To show the details about the ARPES mesuarment results, the calculated surface states along the $\bar{K}$-$\bar{\Gamma}$-$\bar{K}$ direction (Fig. S7c) is also presented. Therefore, by ARPES measurement, the existence of non-trivial topological surface states is confirmed in $MnSb_2Te_4/(Sb_2Te_3)_2$.

References

1 Huan, S. C. *et al*. Magnetism-induced ideal Weyl state in bulk van der Waals crystal $MnSb_2Te_4$. *Appl Phys Lett* **118,** 192105 (2021).

2 Huan, S. C. *et al*. Multiple Magnetic Topological Phases in Bulk van der Waals Crystal $MnSb_4Te_7$. *Phys Rev Lett* **126,** 246601 (2021).

3 Murakami, T. *et al*. Realization of interlayer ferromagnetic interaction in $MnSb_2Te_4$ toward the magnetic Weyl semimetal state. *Phys. Rev. B* **100,** 195103 (2019).

4 Ruderman, M. A. & Kittel, C. Indirect Exchange Coupling of Nuclear Magnetic Moments by Conduction Electrons. *Phys. Rev.* **96,** 99-102 (1954).

5 Yosida, K. Magnetic Properties of Cu-Mn Alloys. *Phys. Rev.* **106,** 893-898 (1957).

6 Kasuya, T. A Theory of Metallic Ferro- and Antiferromagnetism on Zener's Model. *Prog. Theor. Phys.* **16,** 45-57 (1956).

7 Hu, C. W. *et al*. Realization of an intrinsic ferromagnetic topological state in $MnBi_8Te_{13}$. *Sci. Adv.* **6,** eaba4275 (2020).